Flow profile near a wall measured by double-focus fluorescence cross-correlation

D. Lumma,[1] A. Best,[1] A. Gansen,[1] F. Feuillebois,[2] J. O. Rädler,[1,*] and O. I. Vinogradova[1,3,†]
[1]*Max-Planck-Institut für Polymerforschung, Ackermannweg 10, D-55128 Mainz, Germany*
[2]*Laboratoire de Physique et Mécanique des Millieux Hétérogènes, ESPCI, 10 rue Vauquelin, 75231 Paris Cedex 05, France*
[3]*Laboratory of Physical Chemistry of Modified Surfaces, Institute of Physical Chemistry, Russian Academy of Sciences, 31 Leninsky Prospect, 117915 Moscow, Russia*
(Received 29 October 2002; published 27 May 2003)

We present an experimental approach to flow profiling within femtoliter sample volumes, which allows the high-precision measurements at the solid interface. The method is based on the spatial cross-correlation of the fluorescence response from labeled tracer particles (latex nanospheres or single dye molecules). Two excitation volumes, separated by a few micrometers, are created by two laser foci under a confocal microscope. The velocity of tracer particles is measured in a channel about 100 μm wide within a typical accuracy of 0.1%, and the positions of the walls are estimated independently of any hydrodynamic data. The underlying theory for the optical method is given for an arbitrary velocity profile, explicitly presenting the numerical convolutions necessary for a quantitative analysis. It is illustrated by using the Poiseuille flow of a Newtonian liquid with slip as an example. Our analysis yields a large *apparent* fluid velocity at the wall, which is mostly due to the impact of the colloidal (electrostatic) forces. This colloidal lift is crucially important in accelerating the transport processes of molecules and nanoparticles in microfluidic devices.

DOI: 10.1103/PhysRevE.67.056313 PACS number(s): 47.15.Gf, 47.80.+v, 83.50.Lh, 83.85.Ei

I. INTRODUCTION

The ability to create structures on micron length scales has triggered a wide range of scientific investigations, as well as the development of many devices to transport and manipulate liquids. These types of investigations are broadly identified under the theme of microfluidics [1,2]. Microfluidics normally refers to devices or flow configuration that have the smallest design feature on the scale of a micron or larger. Frequently, this means rectangular channels with cross-sectional dimension of the order of tens or hundreds of microns. Most of the microfluidic studies have focused on specific microdevices, such as the design of pumps, mixers, reactors, and sensors. However, these studies could have a great impact in many areas of the physics of liquid, chemistry, and biology, and there are many opportunities for a basic physics, as well as interdisciplinary work in this area. Indeed, on the one hand, the flow in the microchannels naturally remains laminar, i.e., falls into a category that is of long interest of hydrodynamic and chemical engineering community. On the other hand, the new research questions and themes introduced by the small length scale are the motion of particles (in the broad sense, including organic molecules, biomolecules, droplets, tiny bubbles, etc.) and the impact of surface phenomena (surface roughness, colloidal interactions, wettability, etc.).

Among the themes to consider are the boundary conditions at the liquid-solid interface, and their role in determining the transport of particles near the wall. It is accepted in hydrodynamics that, at a macroscopic level, the boundary condition for a viscous fluid at a solid wall is one of no slip, i.e., the liquid velocity is equal to that of a solid boundary. The possibility of slip was intensively discussed only in the context of polymer melt flow [3,4]. It was also suggested that surface roughness [5], hydrophobicity [6], and chemical inhomogeneities [7] could lead to an *apparent* slippage of simple liquids on the wall (for a review see Ref. [8]). This issue has seen a renaissance in recent times. These have been mostly indirect experiments, based as before on the measurements of increase of liquid flow rate as compared with predicted in case of no slip [9,10]. New development included a high-speed force measurements performed with the surface force apparatus [11–13] and atomic force microscope [14,15], and subsequent comparison with a theory of film drainage between slippery surfaces [16]. However, there have also been recent attempts of more direct measurements of the flow velocity near a surface including total internal reflection-fluorescence spectroscopy after photobleaching [17] and an optical study [18]. The principal theme of this paper is a direct study of the flow profile near the interface with a solid using a different method, based on spatial fluorescence cross-correlation.

The technique of fluorescence correlation spectroscopy (FCS) [19] has become an important tool for investigating the dynamic properties of single molecules in solution. The method is based on detecting the fluctuations of the fluorescent light intensity in a small and fixed volume element, usually formed by a laser focus of submicron waist size. Due to minimal requirements on sample amounts, FCS has found widespread application to partially labeled, biological materials, probing quantities such as diffusive behavior [20,21], reaction kinetics [22], and intracellular particle concentrations [23]. Due to the small volumes employed, FCS is also destined to yield important results on the flow velocity within microstructures. Standard, single-focus FCS was shown to yield a classical hydrodynamic flow profile within a 50-μm channel [24]. However, measuring flow with a standard FCS setup implies significant disadvantages. First, a

*Present address: Ludwig-Maximilians-Universität, Geschwister-Scholl-Platz 1, D-80539 München, Germany.
†Corresponding author.
Email address: vinograd@mpip-mainz.mpg.de

single-focus setup does not allow one to observe flows slower than diffusion, and the experimental observable is coupled to diffusion. Second, the direction of the flow cannot be determined. Third, flow velocity cannot be measured close to an interface since size of the focus cannot be controlled in the vicinity of an interface.

These disadvantages can be addressed by monitoring the fluorescence signals from two distinct spots. By cross-correlating the two signals, directed flow can be effectively decoupled from diffusion. As the two focal spots approach an interface, they might change shape and size, but their relative distance remains constant. We will show how this enables us to profile the flow velocity in a channel up to fractions of a micrometer near its walls. The idea of spatial cross-correlation has been applied early on to perform single-molecule electrophoresis on solutions of λ DNA [25]. Compared to such a two-point cross-correlation, two-dimensional fluorescence imaging, which may also be used for high-throughput single-molecule screening applications [26], can only access much longer delay times. For the context of classical FCS, the principles of spatial cross-correlation have been formulated in Ref. [27] for constant flow velocities. The corresponding experiments probed the electrophoretic behavior of Rhodamin 6G solutions, and the two sample volumes were created by two glass fibers of 100 μm diameter with a fixed center-to-center distance of 140 μm. Such dimensions make it impossible to probe the flow behavior within biologically relevant structures such as cells.

In this paper, we present an experimental setup allowing us to perform high-precision velocity measurements within a femtoliter sample volume, formed by two diffraction-limited foci with a distance of 6.0 ± 0.1 μm. With our setup, we can directly probe the entire velocity profile within a 110-μm-wide channel. Cross-correlation data are analyzed by taking into account the nonuniform velocity across the focus. The geometry of our experimental setup is illustrated in Fig. 1. Two optically equivalent and diffraction-limited laser foci are separated by a distance Δs along the x axis. Both foci can be scanned together along the z direction. The time-resolved fluorescence intensities $I_1(t')$ and $I_2(t')$ reflect the number of labeled particles present in focus 1 and 2, respectively. Both intensities correspond to the same optical spectrum, but do so at different locations. The flow velocity is assumed to be directed solely along the x axis, with diffusion taking place into all directions. With this setup, we address the question of *apparent* boundary slip at and motion of particles near microchannel walls.

II. THEORY

In this section, we will describe how a velocity profile can be characterized by our cross-correlation data. We will proceed in two steps. First, we will describe the relationship between the local flow velocity profile and the measured FCS cross-correlation function. Second, we will present the functional form compared to the observed flow profile.

A. Spatial fluorescence cross-correlation spectroscopy

The principles of FCS are detailed elsewhere [28]. Briefly, the technique rests on the premise that only a small number

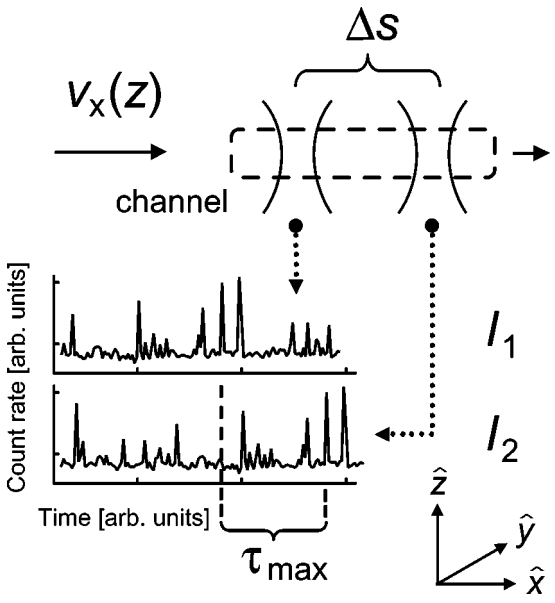

FIG. 1. Geometry of the experimental setup. Two laser foci are placed along the x axis separated by a distance Δs. They independently record the time-resolved fluorescence intensities $I_1(t)$ and $I_2(t)$. The forward cross-correlation of these two signals yields $g_2(t)$. The two foci are scanned simultaneously along the z axis to probe the velocity profile $v_x(z)$.

of labeled particles are simultaneously located in an effective focal volume of the order of 10^{-15} l. For the present experiments, the volume element probed is created by a confocal microscope [29]. Fluctuations of the detected fluorescence signal are due to fluorophors entering or leaving the open illumination volume. The autocorrelation of the time-resolved fluorescence signal permits the characterization of particle concentration and dynamics. Given the size of the effective sample volume, systems with particle concentrations in the range between 10^{-10} and 10^{-6} M may be investigated.

A time cross-correlation function $g_2(t)$ may generally be derived from any two time-resolved intensities $I_1(t')$, $I_2(t')$. It is calculated via

$$g_2(t) = \frac{\langle I_1(t') I_2(t'+t) \rangle_{t'}}{\langle I_1(t') \rangle_{t'} \langle I_2(t') \rangle_{t'}}, \tag{1}$$

with $\langle \cdots \rangle_{t'}$ denoting the ensemble average for an ergodic system. In the present FCS experiment, the quantity $I_n(t')$ is given by the fluorescence intensity detected by focus n at time t'. The shape of the measured cross-correlation versus delay time may be derived from

$$g_2(t) = \frac{\int\int i_1(\vec{r}) i_2(\vec{r}') \Phi(\vec{r},\vec{r}',t) d^3\vec{r} d^3\vec{r}'}{\overline{C}^2 \int\int i_1(\vec{r}) i_2(\vec{r}') d^3\vec{r} d^3\vec{r}'} \tag{2}$$

where $\vec{r} = (x,y,z)$ and $\vec{r}' = (x',y',z')$. The average concentration of labeled particles is denoted by $\overline{C}$ and the functions

$i_n(\vec{r})$ refer to the real-space detection efficiencies for focus n. The latter are modeled as three-dimensional, ellipsoidal Gaussians with cylindrical symmetry about the z axis,

$$i_n(\vec{r}) = \kappa_{0n} \exp\left[-\frac{2(x-x_{cn})^2 + 2y^2}{r_0^2} \right] i_{0n}(z) \times \exp\left[-\frac{2(z-z_c)^2}{z_0^2} \right], \quad (3)$$

with r_0 the waist size of the focus, z_0 its height, and κ_{0n} an excitation- and tracer-specific detection parameter for focus n. The functions $i_{0n}(z)$ are used to reflect the change in the local tracer concentration with z. In our experiments, the $i_{0n}(z)$ are assumed to be proportional to the measured average intensity of focus n at center position z.

The detection efficiency $i_n(\vec{r})$ of focus n is centered about the position $(x_{cn},0,z_c)$ in real space. In our geometry, $x_{c1}=0$ and $x_{c2}=\Delta s$, so that the two foci are displaced by the distance Δs along the x axis. The dynamics of the system is determined through $\Phi(\vec{r},\vec{r}',t)$, denoting the space-time correlation function of a single labeled particle. For a three-dimensional Brownian walk with diffusion constant D, superposed to a uniform flow velocity $\vec{v}=(v_x,v_y,v_z)$, the function $\Phi(\vec{r},\vec{r}',t)$ is solution of an advection-diffusion equation. Such an equation takes into account the Taylor dispersion, that is the larger dispersion along streamlines due to the Brownian diffusion across streamlines in a shear flow. Some solutions of the advection-diffusion equation and estimates of Taylor dispersion are discussed in Appendix A. Here, for the sake of simplicity of the subsequent analysis, we only take the solution of the diffusion equation with a change of frame of reference. Consequences of this simplification are discussed in Appendix A and below. Thus, we take the standard solution

$$\Phi(\vec{r},\vec{r}',t) = \overline{C}(4\pi D t)^{-3/2} \exp\left[-\frac{(\vec{r}-\vec{r}'+\vec{v}t)^2}{4Dt} \right]. \quad (4)$$

In our experiments, $\vec{v}=(v_x,0,0)$, and $v_x=v_x(z)$. With these assumptions, we may simplify Eq. (2) to obtain

$$g_2(z_c,t) = 1 + N^{-1}(1+4Dt/r_0^2)^{-1} z_0^{-1} \times \int_{-L}^{+L}\int_{-L}^{+L} \hat{i}_{01}(z)\hat{i}_{02}(z') \exp\left[-\frac{2(z-z_c)^2}{z_0^2} \right] \times \exp\left[-\frac{2(z'-z_c)^2}{z_0^2} \right] (4\pi D t)^{-1/2} \times \exp\left[-\frac{(z-z')^2}{4Dt} \right] \exp\left\{ -(1+4Dt/r_0^2)^{-1} \times \frac{[\Delta s - v_x(z)\,t]^2}{r_0^2} \right\} dz\,dz', \quad (5)$$

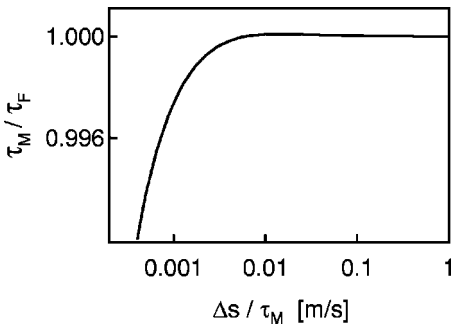

FIG. 2. The deviation between τ_M and τ_F. The ratio τ_M/τ_F is plotted versus the velocity $\Delta s/\tau_M$.

where $\hat{i}_{0n}(z) = i_{0n}(z)[\int_{-L}^{+L} i_{0n}(z'')dz'']^{-1}$. The number $N = \overline{C}V_{\rm eff}$ denotes the average number of particles present within a focus, where

$$V_{\rm eff} = \int_{-\infty}^{+\infty}\int_{-\infty}^{+\infty}\int_{-L}^{+L} \exp\left[-\frac{2(z-z_c)^2}{z_0^2} \right] \times \exp\left[-\frac{2(x-x_{cn})^2+2y^2}{r_0^2} \right] dx\,dy\,dz \quad (6)$$

refers to the effective focal volume. In the simple case of $L\to\infty$ where the wall is far away, one finds $V_{\rm eff}=\pi^{3/2} z_0 r_0^2$. The position $z=0$ is defined as the center of the channel, and integration is performed between the walls at $z=+L,-L$. In the limit $L\to\infty$, $\Delta s=0$, $v_x=0$, and $\hat{i}_{01}=\hat{i}_{02}=1$, Eq. (5) reduces to

$$g_2(t) = 1 + g_{\rm diff\,3D}(t) = 1 + N^{-1}(1+t/\tau_D)^{-1}[1+t/(S^2\tau_D)]^{-1/2}, \quad (7)$$

describing the three-dimensional Brownian diffusion with $D=0.25\,r_0^2/\tau_D$ [19] and $S=z_0/r_0$. In the case of plug flow, where $v_x\neq 0$ is independent of z and $\hat{i}_{01}=\hat{i}_{02}=1$, Eq. (5) simplifies to

$$g_2(t) = 1 + N^{-1}(1+t/\tau_D)^{-1}[1+t/(S^2\tau_D)]^{-1/2} \times \exp\left\{ -(1+t/\tau_D)^{-1} \frac{(\Delta s - v_x t)^2}{r_0^2} \right\}, \quad (8)$$

as in Ref. [27]. The results quoted here are strictly valid for pointlike particles only, but remain applicable to particles with radius R significantly smaller than the focal waist size r_0 (Fig. 2). As particle radii become comparable to the focal waist size r_0, the relationship between the diffusion time τ_D and the diffusion constant changes to $D=0.25(r_0+R)^2/\tau_D$ [30]. In the experiments presented here, $R \ll r_0$.

B. Flow velocity profile

In the preceding section, we have outlined how to model the expected cross-correlation function given an arbitrary flow profile $v_x(z)$. We will now describe our model for the

underlying velocity profile itself. In this paper, we illustrate our approach by considering the Poiseuille flow with slip boundary conditions. In other words, we allow an amount of slippage, described by a slip length b

$$v_s = b\frac{\partial v_s}{\partial n},$$

where v_s is the slip (tangential) velocity on the wall and the axis n is normal to the surfaces. In such a model, the slip velocity of the wall is proportional to the shear stress [8].

Therefore, we begin with a general solution of the Navier-Stokes equations

$$v_x(z) = Az^2/2 + c_1 + c_2 z, \tag{9}$$

where $A = \mu^{-1} dP/dz$ with μ the bulk viscosity of the medium and P the hydrostatic pressure. The two constants c_1, c_2 are then determined from the set of boundary conditions

$$\mp b_{1,2}(c_2 \pm AL) = c_1 \pm c_2 L + AL^2/2, \tag{10}$$

The quantities b_1, b_2 denote the slip lengths for the upper and lower channel wall located at $z = +L$ and $z = -L$. The pressure drop measurements cannot be performed with the necessary accuracy. However, one can express the pressure drop via a velocity in the center of the channel, which we consider to be independent of the slip situation at the walls. The last assumption is justified provided $b_1, b_2 \ll L$. We therefore use $v_0 \sim -AL^2/2$ and obtain

$$v_x(z) = \frac{v_0}{L^2(b_1 + b_2 + 2L)}\{b_1(4b_2 L + 3L^2 + 2Lz - z^2) + (L - z)[2L(L + z) + b_2(3L + z)]\}, \tag{11}$$

which reduces to the symmetric form

$$v_{x\,\mathrm{symm}}(z) = v_0 \frac{2bL + L^2 - z^2}{L^2} \tag{12}$$

in the limit where $b_1, b_2 \to b$.

Using the profile $v_x[v_0, L, b_1, b_2](z)$ from Eq. (11), we can calculate the expected FCS cross-correlation function $g_2[v_0, L, b_1, b_2](t)$ by means of Eq. (5), and by assuming that the velocity of particles we measure is equal to that of liquid flow. This cross-correlation will typically exhibit a local maximum whose position τ_M is characteristic of the local flow velocity. In order to efficiently compare the theoretical expectation to the measured data, we locally perform a least-squares fit of

$$g_2(t) = b + H\exp\left[-\frac{(t - \tau_M)^2}{w^2}\right] \tag{13}$$

to the calculated $g_2[v_0, L, b_1, b_2](t)$.

III. EXPERIMENTAL METHODS

Fluorescently labeled latex spheres, carboxylate-modified FluoSpheres (580/605), were purchased from Molecular Probes (Eugene, Oregon) and provided in a solution with 2% solids. The particles are specified to have a radius of $R \simeq 20$ nm and a polydispersity of about 20%. The suspension was diluted by 1:10 000, and steps were undertaken to prevent aggregation. As long as R remains significantly smaller than the focal waist size r_0, neither the exact size of the particles nor their polydispersity affects the measured flow profiles. The tracers were solely chosen for their ease to use and their fluorescence brightness. Measurements with single dye molecules were performed with Alexa 568 (Molecular Probes) at a final concentration of 2 nM.

Experiments were carried out in water and NaCl (99.99%, Aldrich) aqueous solutions with concentrations in the range between 0.01 mM and 0.1M. Water was purified using a commercial milli-Q system containing ion-exchange and charcoal stages. The deionized water had a conductivity less than 0.1×10^{-6} S/m. It was filtered at 0.22 μm and degassed before use to minimize air bubble formation during the measurements. All experiments were done at room temperature without buffer. Hence, pH was around 6.

We use a commercial FCS setup manufactured by Carl Zeiss (Jena, Germany) consisting of the module ConfoCor 2 and the inverted microscope model Axiovert 200. For the present experiments, we employed a Zeiss Plan-Neofluar 40× water immersion objective. The optical system was modified by the manufacturer such that an external laser beam could be coupled into the confocal optics. For fluorescence excitation, the 543-nm line of a 5-mW helium-neon laser is used. The laser beam is split by means of a Wollaston prism. Behind the prism, the two beams are polarized perpendicularly to each other and exhibit an angular separation of 0.5°. The prism is followed by two lenses, the first with a focal length of 400 mm located at a distance of 380 mm behind the prism. The second lens, with a focal length of 600 mm, is placed 920 mm further downstream. The distance from the second lens to the external input of the ConfoCor 2 system measures about 680 mm. Our alignments lead to two optically equivalent, almost diffusion-limited laser foci separated by a distance of 6.0 ± 0.1 μm in object space.

Emitted fluorescence was separated from the laser source with a dichroic mirror adjusted to the 543-nm line. The light passing the dichroic was evenly split to enter the two independent channels using a neutral 50:50 beam splitter. The emission pinholes before the two detectors were carefully centered on the intensity maxima corresponding to the spatially separated excitation volumes. In both channels, filters were chosen to allow only light at wavelengths longer than 585nm to enter the detectors. For detection, avalanche photodiodes were used, enabling single-photon counting. After proper alignment, the photon cross talk between channels did not exceed 4.5%.

For calibration, an aqueous solution of 10 nM Rhodamin 6G (R6G) was studied before each data acquisition series, and the autocorrelations were fitted to

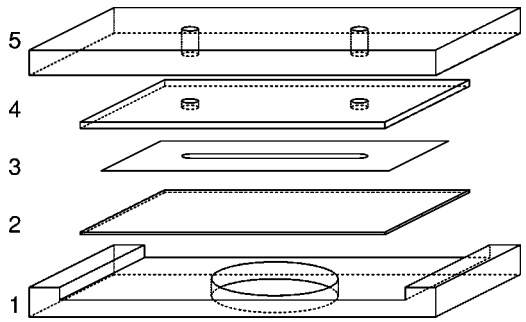

FIG. 3. Schematic of the chamber: 1—aluminium support, 2—cover slide, 3—thermoplastic foil, 4—microscope slide, 5—polycarbonate block.

$$g_2(t) = 1 + g_{\mathrm{tr}}(t) g_{\mathrm{diff\,3D}}(t), \tag{14}$$

with $g_{\mathrm{tr}}(t) = [1 + e^{-t/\tau_{\mathrm{T}}} T/(1-T)]$ accounting for the triplet decay [31]. With the R6G diffusion constant $D_{\mathrm{R6G}} = 2.8 \times 10^2\ \mu\mathrm{m}^2\,\mathrm{s}^{-1}$ [28] as a reference, the focal waist size and shape parameter were determined ($r_0 \simeq 0.21\ \mu$m and $S = z_0/r_0 \simeq 7.7$) and used for all subsequently acquired data. Flow experiments were only carried out when the size of the two foci did not deviate by more than 15%. Experiments confirmed that the measured autocorrelations for R6G solutions were independent of laser intensity for attenuator transmissions up to 5%. Beyond 2%, distortions appear. All R6G measurements for the present work were performed at attenuator transmissions between 0.5% and 2%.

The surfaces used for our measurements have been characterized by their contact angle and morphology. The measurements of water contact angle were done by observation of a sessile drop with a commercial setup (DataPhysics, Germany) equipped with a stepper motor to drive the syringe which controls the drop volume. The estimated error is roughly $\pm 1°$. The imaging of surface topography was done with a commercial AFM (NanoScope III, Multimode, Digital Instruments, California).

The chamber within which the flow was profiled is formed by a three-layer sandwich construction (Fig. 3). Before use, all the surfaces were cleaned with plasma treatment. The lowest layer is a standard microscope cover slide made of borosilicate glass with a height of 170 μm, a root-mean-square roughness of the range 2.5–3 nm and with a maximum peak-to-valley difference of the order of 15 nm. The water advancing contact angle was found to be 5–10°. The channel itself was created by a polymer film (Xiro, Schmitten, Switzerland). The height of this film, roughly 110 μm, also forms the smallest dimension of the channel, directed along the *z* axis. The channel extension along the *y* axis is cut out of the film, and measures about 1.5–2 mm. The top layer is finally formed by a 1-mm-thick cover glass (Menzel, Germany). Experiments involving mica were performed by introducing a freshly cleaved thin (usually 5–10 μm) piece of molecularly smooth mica between the polymer film and the upper glass slide. Two holes were made in this upper cover glass directly on top of the channel ends. The holes work as entry and exit for the fluid. Heating under gentle pressure causes the film to stick to the upper and lower glass plates, sealing the system. An optically transparent polycarbonate block served as a support and for connection of the chamber to the external flow system.

A hydrostatic pressure gradient was created by a system of two beakers at different heights. Liquid then flows from the upper to the lower beaker at a height-dependent volume rate. Prior to our data on flow profiles, we have performed a simple calibration test that included the measurements of flow velocity at some fixed point far from the walls. Measurements verified the linear relation between velocity and pressure drop to very high accuracy. The surface area of both beakers was chosen large enough to minimize the change in height difference between the two fluid surfaces during the experiment. Since this change affects the rate of liquid passing through the channel a correction to the flow data has to be applied, which accounts for the hydrostatic pressure drop during the experiment. To obtain a characteristic time constant of the system, the temporal change of flow velocity was monitored at a given position inside the channel. In good agreement with theoretical expectations, the flow velocity followed an exponential dependence on time. For a typical initial height difference of 30 cm a time constant of $\tau = (44.28 \pm 0.22)$ h was observed. For typical durations of 6–8 h per channel scan, this exponential behavior can be approximated by a linear correction $v(t) = v_{\mathrm{measured}}(t)/(1 - t/\tau)$.

Measurements on the latex tracers and single dyes were done at attenuator transmissions up to 2%. Before each flow experiment, the self-diffusion of the particles was characterized. For the latex particles, the triplet decay turned out to be negligible, and we assumed $g_{\mathrm{tr}}(t) = 1$. The flow profile was determined by calculating the cross-correlation, as well as the two autocorrelations simultaneously, while the data were being accumulated. At each *z* position, a series of at least five independent data acquisitions was carried out. The acquisition time was varied to yield sufficient signal-to-noise ratios at each position, necessitating longer measurements close to the channel walls, where small flow velocities are found. Longest data acquisition times reached about 90s. The independent cross-correlation functions acquired at position *z* were fitted to Eq. (13), yielding the experimental flow velocity $v_{\mathrm{exp}}(z) = \Delta s/\tau_{\mathrm{Mexp}}$, as well as the height $H_{\mathrm{exp}}(z)$ and width $w_{\mathrm{exp}}(z)$ of the Gaussian for position *z*. Statistical uncertainties were determined by calculating the standard deviation from the variation among the independent measurements.

Figure 4(a) illustrates how the position of the two walls may be determined independent of any hydrodynamic data. We show the product of the average intensities detected by the two foci, plotting $I_1 I_2$ vs the focal center position z_{c}. Well within the channel, we observe a symmetric curvature. As z_{c} approaches the walls, the product $I_1 I_2$ decreases, and vanishes a few micrometers outside the channel. One may consider the walls to be located where the derivative of $I_1 I_2$ with respect to z_{c} reaches an absolute local maximum. An alternative approach uses the cross-correlation data to estimate the wall locations. In panel (b), we plot the area under the peak of the measured cross-correlation as a function of z_{c}. This area F is proportional to wH in Eq. (13). It is evident that F is peaked near the wall positions since diffusive

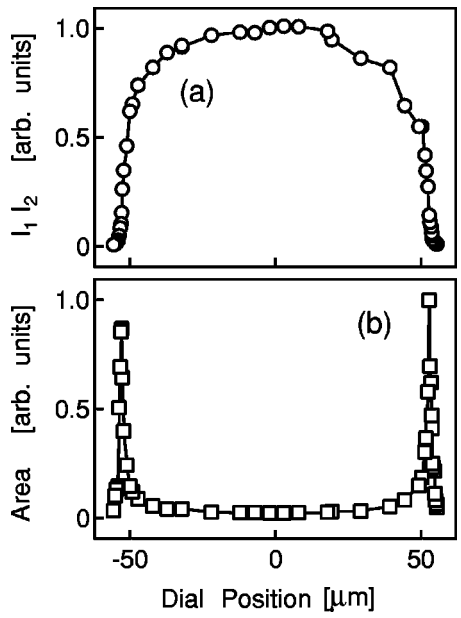

FIG. 4. Procedure for estimating the wall positions. (a) The product of the average intensities detected by the two foci, plotting $I_1 I_2$ vs the focal center position z_c. (b) Area $F \propto wH$ in Eq. (13) under the peak of the measured cross-correlation, plotted vs z_c.

broadening is most pronounced where local flow velocities are smallest. This position was determined by fitting the peaked region to a Lorentzian function. This lead to estimates for the wall positions that agree to within ± 0.1 μm, which is of the order of the step width between successive scan positions. In addition, they are also consistent with the fits to the velocity profile that will be described below. However, we want to stress that this procedure does not represent a direct measurements of the wall position.

Additional problems may arise from the appearance of air bubbles in the channel structure due to imperfect sealing of the flow system. Small bubbles stuck to the wall will diminish the flow velocity near the surface by changing the effective cross section of the channel. Although careful steps were undertaken to minimize this disturbance, the effect was visible in the deformation of the parabolic profile, especially for prolonged measurements. Data showing distortions near the walls were discarded from further analysis.

The measured cross-correlation data were compared to theory as follows. On the basis of the parameters v_0, L, b_1, b_2, we calculate a velocity profile from Eq. (11), which in turn yields the expected correlation function $g_2(z,t)$ from Eq. (5). Through a fit to Eq. (13), we finally obtain $\tau_{\mathrm{M\,mod}}[v_0, L, b_1, b_2]$ as a prediction for the experimentally observable τ_{Mexp}. Performing least-squares fits of $v_{\mathrm{mod}}[v_0, L, b_1, b_2](z) = \Delta s / \tau_{\mathrm{M\,mod}}$ to $v_{\mathrm{exp}}(z)$, we obtain the slip lengths b_1, b_2, the center velocity v_0, and an independent verification of the channel half width L.

IV. RESULTS AND DISCUSSION

Representative cross-correlations $g_2(z,t)$ are shown in Fig. 5. Panel (a) shows data from well within the channel. As the flow becomes slower, the peaks in the cross-correlation

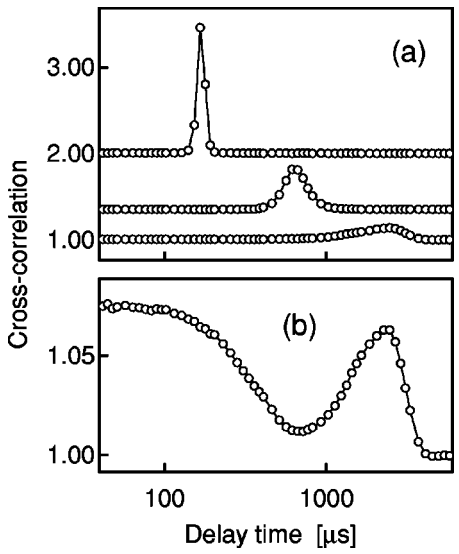

FIG. 5. Cross-correlation functions $g_2(z,t)$ vs delay time (a) for positions well within the channel and (b) for measurements very close to the walls. Two of the baselines in (a) were offset from 1.0 for presentational purposes.

lose in height and gain in width. These findings are in agreement with Eqs. (5) and (8). Panel (b) shows a cross-correlation for a measurement close to the channel wall, where diffusion and transport occur at similar time scales. The overall velocity profile within the entire 110-μm-wide channel is shown in Fig. 6. The solid line is a least-squares fit to the model of Eqs. (5), (11), and (13). The absolute uncertainty of the measured velocities is on an average 2.5×10^{-4} m s^{-1} and shows only a weak dependence on the mean velocity. For all data points, the fitted model lies within the experimentally determined uncertainties. Within the central 2/3 of the channel, we find characteristic relative statistical errors down to 0.06%. The fit yields $v_0 = (0.0854 \pm 0.0001)$ m s^{-1} and $L = (52.56 \pm 0.04)$ μm. As expected, the central region of the profile exhibits the parabolic shape

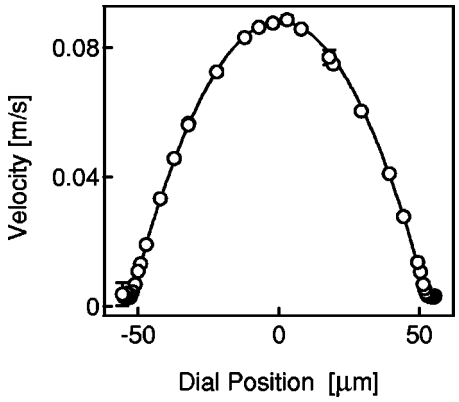

FIG. 6. Typical observed velocity profile $v_{\mathrm{exp}}(z)$ within a 110-μm-wide channel. The solid lines are curvefits to the model of Eqs. (5), (11), and (13), presenting $v_{\mathrm{mod}}[v_0, L, b_1, b_2](z) = \Delta s / \tau_{\mathrm{M\,mod}}$. Error bars were determined from the deviation among repeated measurements. When error bars are absent, uncertainties are smaller than the circles.

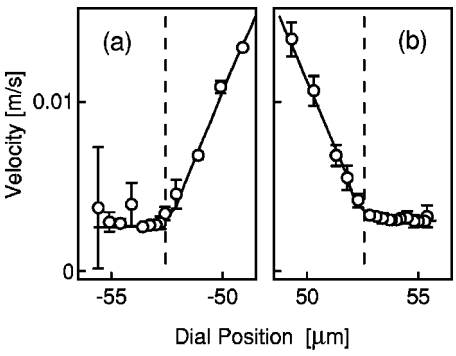

FIG. 7. Observed velocity profile $v_{\mathrm{exp}}(z)$ in the vicinity of the channel walls at $\pm L$. The solid lines are curve fits to the model of Eqs. (5), (11), and (13), presenting $v_{\mathrm{mod}}[v_0,L,b_1,b_2](z) = \Delta s/\tau_{\mathrm{M\,mod}}$. Error bars were determined from the deviation among repeated measurements. When error bars are absent, uncertainties are smaller than the circles. The dashed lines show the fitted position of the channel walls. Determining wall positions as described in the text, fits yield slip lengths of (a) $b_1=(0.89 \pm 0.02)$ μm and (b) $b_2=(0.77\pm 0.03)$ μm.

that is predicted by the classical theory. An important point to note is that our method provides a much higher space resolution in the velocity measurements than the classical single-focus FCS [24] or state-of-the-art confocal imaging studies using particle tracking [32]. This remains true even far from interfaces. Similarly, these other methods may not reach flow times as short as those accessible with spatial double-focus cross-correlation.

The parabolic shape, however, does not extend up to the channel walls, as shown in Fig. 7. As the center position of the two foci approaches the location of the wall and leaves the interior of the channel, the measured velocity converges towards a constant value. This behavior can be explained intuitively. As the two focal spots approach an interface, their relative distance remains constant despite possible changes in shape. Once the centers of the two foci lie outside the channel, only fractions of the sampling volume, specifically the tails of the Gaussians in Eq. (3), will remain within the channel. The velocity effectively quantified through τ_{M}^{-1} will thus correspond to a weighted average velocity belonging to that tail region. As we continue to scan the two foci into the wall, the measured flow should converge to just that velocity that is effective in the last moving particle layer close to the wall.

Our model also allows us to accurately fit the experimental data near the walls. This means that the continuum description with the appropriately chosen slip lengths remains an appropriate starting point for analysis of flow near the walls of a microchannel. Therefore, we can determine the *apparent* slip lengths quantitatively. For the shown profile (glass and borosilicate glass in water) the fits yield $b_1 =(0.89\pm 0.02)$ μm and $b_2=(0.77\pm 0.03)$ μm. The results for different experimental situations are summarized in Table I. The data given there represent average values of roughly 20 profiles taken in each case. For every measured profile, the fit has given values of the slip length with the uncertainty below ± 0.03 μm. However, the scatter in the average values of slip lengths measured in the same conditions in separate experiments was much larger (up to ± 0.1 μm in case of pure water). Data obtained at higher concentration of electrolyte are not presented in Table I. The reason is that in concentrated solutions the tracers themselves get stuck at the wall giving rise to a high uncertainty in the measured values. Therefore, they have been excluded from further analysis.

TABLE I. Average *apparent* slip lengths (micrometers) at various conditions for the different surfaces.

Condition	Borosilicate glass slide	Glass slide	Mica
Latex spheres Salt-free	1.00	0.89	0.86
Alexa 568 Salt-free	0.82	0.63	0.51
Alexa 568 0.01 mM salt	0.32	0.59	
Alexa 568 1 mM salt	0.25	0.22	

The essential observations are these. The apparent slip lengths measured with the latex tracers in water have very large values (of the order of 1 μm). These values are well above the size of asperities of the microchannel walls and independent of the nature of the surfaces. The use of smaller size dye molecules leads to a reduction of the apparent slip length. With the added electrolyte further reduction is observed. These findings require further comments.

Clearly, the apparent slip lengths we found are too large to reflect just the liquid slippage over the wall, especially taking into account that we had a nearly complete wetting situation. The possible explanation could be connected with the fact, that in reality, we do not measure the fluid velocity v_x itself, but the velocity u_x of particles carried by the fluid.

One reason for such differences between these two quantities may be connected with the influence of hydrodynamic interactions of spheres with walls. This can be estimated on the basis of classical results (reviewed in Ref. [33]; cf. also Ref. [34] for the shear flow problem).

Due to its small radius $R\sim 20$ nm (or even smaller in case of dye molecules), a marker may be regarded as neutrally buoyant. When a sphere is located in the central part of the channel in a Poiseuille flow, wall interactions are of the order of $(R/L)^2\sim 10^{-8}$. The same is true for slip walls, since we may use the remark that the fluid velocity in a channel with slip boundary conditions on the walls is equivalent to a Poiseuille flow displaced by a distance equal to the slip length b. Interactions with walls only become important when a sphere is in the vicinity of either wall, at distances of about $20R=0.4$ μm and less. For such distances, it is clear that the flow profile close to either wall is practically a shear flow.

Consider then a freely moving, freely rotating sphere in a shear flow in the vicinity of a plane wall. First, for a no-slip wall ($b=0$), the sphere velocity is 0.96 of the fluid velocity when the normalized gap ϵ between the sphere and the wall is unity and 0.76 when $\epsilon=0.1$. Thus, if the fluid velocity at distances of the order of 0.04 μm or less is to be measured close to a no-slip wall, the sphere-wall hydrodynamic inter-

actions have to be included in the analysis. Since these distances are much shorter than the apparent slip lengths that we observed, this simple effect can be eliminated. Consider now a sphere close to a wall on which a slip condition applies. To our knowledge, this creeping flow problem was not solved; so we use an approximate solution, as detailed in Appendix B. In the range of validity of this solution, that is, for $b \geqslant 5R = 0.1$ μm, the fluid and particle velocity are practically equal. For smaller gaps, the theory is missing but some difference between the particle and fluid velocity close to a slip wall could be anticipated.

Another possible reason for a large apparent slip we observe could be particle depletion within a layer close to the microchannel walls. The depletion due to hydrodynamic lift has been observed for a layer thickness between 0.3 and 1.4 μm [35]. We should, however, rule out a possibility for a hydrodynamic lift in our system, since such an effect is due to fluid inertia. More precisely, the ratio of the migration velocity due to such a lift to the fluid entrainment velocity is of the order of the Reynolds number based on the shear flow around a particle [36], which is less than 10^{-6} in our case.

We, therefore, conclude, that the depletion layer, if any, can only be caused by repulsive interaction of our tracer particles with the channel walls [37]. The approximate size of such a layer d can be estimated by assuming that it is of the order of the distance from the wall, where there a double layer force $F \propto R\exp(-\kappa d)$ becomes negligibly small (here κ is the inverse Debye length). This happens roughly at $d \sim 3\kappa^{-1}$, and gives $d \sim 0.03$ μm for 1 mM, and 0.3 μm for 0.01 mM solution of NaCl. In water the Debye length is not well defined, but normally it can take it roughly equal to 0.3 μm [38], which suggests d is about 0.9 μm for a pure water. These values are consistent with the apparent slip lengths summarized in Table I. In such an approach, the difference between experiments with nanoparticles and single dyes reflects the difference in the size of the tracers. Also, the influence of the material of the walls on the slip lengths could be connected with the different surface potential (of mica, glass, and borosilicate glass), which determines the strength of the double layer interaction [38,39].

Some discrepancies between the estimated d and the experimental values of slip at concentration 1 mM are likely connected with the simplification we introduced by using the standard solution of the diffusion equation (4). The error may be evaluated on the basis of the Taylor dispersion of particles estimated in Appendix A. If hydrodynamic and colloidal interactions between the particles and wall are neglected, these estimates give slip length consistent with the last line in Table I. An important point to note is that, when particles are repelled from the wall by electrostatic forces, the Taylor slip is much smaller, so that it does not affect our conclusion about the large slip lengths at low salt concentration.

In summary, we have developed an experimental approach, based on the spacial fluorescence cross correlation of the fluorescence response from tracer nanoparticles, which allowed the high-precision flow profiling at the solid interface. The experimental study of a flow of water-electrolyte solutions has shown that there is a significant slip on the wall. We have demonstrated that it would be wrong to interpret this as an actual slip at the liquid-solid interface. This large slip effect is shown to be *apparent*, mostly reflects a colloidal (repulsive) interaction of the tracer particles with the microchannel walls, and can be controlled by varying the concentration of electrolyte. We have provided an accurate quantitative description of the phenomenon using simple physical models, which allows one to control, manipulate, and dramatically accelerate the transport processes, in particular, the motion of molecules and nanoparticles in small devices. To the best of our knowledge, we do so for the first time in this field of study that sees so much attention by numerous communities of scientists.

ACKNOWLEDGMENTS

We thank Dr. V. Jüngel of Carl Zeiss (Jena, Germany) for his continued expert advice, S. Keller for his help with the optical alignment, and V. V. Lulevich for imaging the topography of the surfaces. We are also grateful to R. Sahoo and Dr. G. E. Yakubov for their helpful efforts.

APPENDIX A: ESTIMATES OF TAYLOR DISPERSION

Function $\Phi(\vec{r},\vec{r}',t)$ should satisfy the advection-diffusion equation

$$\frac{\partial \Phi}{\partial t} + \vec{v}\cdot\nabla\Phi = D\nabla^2\Phi. \tag{A1}$$

We use this equation to describe the release at time t and position $\vec{r}'$ of a species initially concentrated at position $\vec{r}$, viz., with initial condition

$$\Phi(\vec{r},\vec{r},0) = \delta(\vec{r}), \tag{A2}$$

where δ is the Dirac delta function. Appropriate boundary conditions of zero flux across the walls should be added. This is the dispersion problem pioneered by Taylor [40]. In Taylor's approach, the dispersed species is filling the whole channel. However, in our case, the distance between foci is 6 μm whereas the distance between channel walls is 100 μm, so that the species usually does not have time to diffuse laterally to the walls in the travel from one focus to the other. An exception is when both foci are close to a wall. Both cases will be considered here.

First, for both foci at some distance from walls, the boundary conditions are dropped. The important phenomenon is the dispersion due to the velocity gradient and we take $v_x = kz$, $v_y = v_z = 0$ in Eq. (A1). The solution of Eq. (A1) with Eq. (A2) then is found to be

$$\Phi = \Phi_0 \frac{1}{\sqrt{1+k^2t^2/12}} \exp\left[\frac{(X^2-3Z^2)k^2t^2/12 + XZkt}{4Dt(1+k^2t^2/12)}\right], \tag{A3}$$

where

$$X = x' - x - kzt, \quad Y = y' - y, \quad Z = z' - z,$$

where Φ_0 denotes here the classical solution (4) for pure diffusion. When the distance y to the wall becomes of the

order of the distance $x'-x=6\ \mu$m between foci and larger, we then calculate with our physical values of parameters that $\Phi \simeq \Phi_0$ so that approximation (4) is quite good enough. This is because far from walls, lateral diffusion does not have time to evolve during the rapid travel from one focus to the other.

Consider now the case when both foci are close to a wall. Obviously, the influence of the other wall will be negligible from the preceding analysis. For this case, we use Saffman's [41] solution for the source on the wall. Although the problem of a source close to the wall considered here is more general, Saffman's solution [see Eq. (25) in Ref. [41]] provides us with an estimate. Since particles released near the wall can only diffuse away from the wall, say at a distance $\sqrt{Dt}$ during time t, they are carried downstream at a larger velocity by the ambient shear flow, viz., $k\sqrt{Dt}$, to an average distance $kt\sqrt{Dt}$. In his exact calculation, Saffman find that this quantity should be multiplied by $\sqrt{\pi}/2$. The velocity $(\sqrt{\pi}/2)k\sqrt{Dt}$ thus is the supplementary velocity observed in the experiment. For simplification, we estimate time t as the fluid transportation time between foci (instead of the particle transportation time). Considering the case when the distance $x'-x$ between foci equals the distance ζ between the foci and the walls, the *apparent* slip velocity is found to be $v_T=\sqrt{\pi Dk}/2$, leading to an *apparent* slip length of $b_T=v_T/k=0.2\ \mu$m. This is of the order of the values found in the last line in the table. When the foci are closer to the wall, this apparent slip length increases like $\sqrt{(x'-x)/\zeta}$. Note, however, that the repulsive interactions between the particles and the wall, which are not taken into account in this analysis, may hinder the particle motion so that the estimated slip length would not be as large.

Saffman's Eq. (25) also gives the dispersion around the average displacement. From that formula, we find that the ratio of the Saffman's dispersion to the Brownian dispersion is $\sqrt{c(x'-x)^2/\zeta^2+1}$, where $c=7/60-\pi/32\simeq 0.0185$. For $(x'-x)/\zeta=1$, we obtain 1.009 and for $(x'-x)/\zeta=0.1$, 1.68. Thus, there is no large experimental error in using the diffusion equation instead of the advection-diffusion one.

APPENDIX B: APPROXIMATE SOLUTION FOR A SPHERE IN A SHEAR FLOW CLOSE TO A PLANE WITH A SLIP BOUNDARY CONDITION

Consider a freely moving, freely rotating sphere in a shear flow, with center at a position $\zeta=l$ away from a plane wall P_s at $\zeta=0$, on which a slip condition applies. For a shear flow without sphere, the slip condition is equivalent to applying the no-slip condition on a plane $\zeta=-b$. We then consider the flow field around the freely moving, freely rotating sphere in presence of this no-slip plane. However, this new problem is not exactly equivalent to the one that we want to solve. This is because the flow calculated in this way gives *a priori* a velocity w across the plane at $\zeta=0$, which is in contradiction with the required boundary conditions on P_s. Nevertheless, if the slip length is large compared with the sphere radius, this equivalence of boundary condition may be good enough. To demonstrate this point, we calculate the velocity across the plane at $\zeta=0$ and compare it with the sphere velocity.

By linearity of the creeping flow equations, the problem of a freely moving, freely rotating sphere is written as a sum of three problems: a sphere translating without rotation (i) and rotating without translation (ii) in a fluid at rest; (iii) a sphere held fixed in a shear flow. These problems were solved by the technique of bipolar coordinates: the first two ones by O'Neill and co-workers in a series of papers (quoted in Ref. [33]) and the last one in Ref. [34]. Taking $b/R=80$ from experiment, calculations made on the basis of these results show that the sphere translational velocity is the same as the unperturbed fluid velocity in its center, with a 10^{-7} precision. When calculating the fluid velocity w across the plane $\zeta=0$ for various values of the normalized distance l/R and of the normalized abscissa ξ/R, the maximum value w_m of $|w|$ is found to be at a maximum around $\xi/R=0.75$. It slowly increases for decreasing gap $\epsilon=l/R-1$, with values $w_m=4\times10^{-3}$ for $\epsilon=0.1$ and $w_m=4.2\times10^{-3}$ for $\epsilon=0.01$. On the basis of the preceding results, we thus find that the sphere translational velocity close to the slip plane is the same as the unperturbed fluid velocity in its center, with a 10^{-7} precision.

The theory by Hocking [42] considers the translation and rotation of a sphere close to a plane with a slip condition and his result for the case of a large slip length leads to results consistent with our simplified model. However, Hocking did not treat the shear flow problem.

For lower values of b, w_m increases as expected. It is 0.05 for $b/R=5$. Thus, $b=5R=100$ nm is about the lower value of the slip length for which the present model is valid. For lower slip lengths, the creeping flow problem of a sphere moving parallel to a slip plane should be solved for better precision.

[1] N. Giordano and J.T. Cheng, J. Phys.: Condens. Matter **13**, R271 (2001).
[2] H.A. Stone and S. Kim, AIChE J. **47**, 1250 (2001).
[3] P.G. de Gennes, C. R. Acad. Sci., Ser. B **288**, 219 (1978).
[4] F. Brochard and P.G. de Gennes, Langmuir **8**, 3033 (1992).
[5] S. Richardson, J. Fluid Mech. **59**, 707 (1973).
[6] N.V. Churaev, V.D. Sobolev, and A.N. Somov, J. Colloid Interface Sci. **97**, 574 (1984).
[7] A.A. Alexeyev and O.I. Vinogradova, Colloids Surf., A **108**, 173 (1996).
[8] O.I. Vinogradova, Int. J. Min. Process. **56**, 31 (1999).
[9] N.V. Churaev, J. Ralston, I.P. Sergeeva, and V.D. Sobolev, Adv. Colloid Interface Sci. **96**, 265 (2002).
[10] K. Watanabe and H. Udagawa, J. Fluid Mech. **381**, 225 (1999).
[11] R.G. Horn, O.I. Vinogradova, M.E. Mackay, and N. Phan-Thien, J. Chem. Phys. **112**, 6424 (2000).
[12] Y.X. Zhu and S. Granick, Phys. Rev. Lett. **88**, 106102 (2002).
[13] J. Baudry, E. Charlaix, A. Tonck, and D. Mazuyer, Langmuir

17, 5232 (2001).
[14] V.S.J. Craig, C. Neto, and D.R.M. Williams, Phys. Rev. Lett. **87**, 054504 (2001).
[15] O.I. Vinogradova and G.E. Yakubov, Langmuir **19**, 1227 (2003).
[16] O.I. Vinogradova, Langmuir **11**, 2213 (1995).
[17] R. Pit, H. Hervet, and L. Leger, Phys. Rev. Lett. **85**, 980 (2000).
[18] D.C. Tretheway and C.D. Mainhart, Phys. Fluids **14**, L9 (2002).
[19] M. Eigen and R. Rigler, Physica A **91**, 5740 (1994).
[20] R. Rigler, P. Grasselli, and M. Ehrenberg, Phys. Scr. **19**, 486 (1979).
[21] N.G. Walter, P. Schwille, and M. Eigen, Proc. Natl. Acad. Sci. U.S.A. **93**, 12 805 (1996).
[22] D. Magde, E. Elson, and W.W. Webb, Phys. Rev. Lett. **29**, 705 (1972).
[23] P. Cluzel, M. Surette, and S. Leibler, Science (Washington, DC, U.S.) **287**, 1652 (2000).
[24] M. Gösch, H. Blom, J. Holm, T. Heino, and R. Rigler, Anal. Chem. **72**, 3260 (2000).
[25] A. Castro and E.B. Shera, Anal. Chem. **67**, 3181 (1995).
[26] M.R. Shortreed, H. Li, W. Huang, and E.S. Yeung, Anal. Chem. **72**, 2879 (2000).
[27] M. Brinkmeier, in *Fluorescence Correlation Spectroscopy*, edited by R. Rigler and E.S. Elson (Springer, Berlin, 2001), pp. 379–395.
[28] D. Magde, E.L. Elson, and W.W. Webb, Biopolymers **13**, 29 (1974).
[29] R.H. Webb, Rep. Prog. Phys. **59**, 427 (1996).
[30] K. Starchev, J. Zhang, and J. Buffle, J. Colloid Interface Sci. **203**, 189 (1998).
[31] J. Widengren, in *Fluorescence Correlation Spectroscopy* (Ref. [27]), pp. 276–301.
[32] S.A. Koehler, S. Hilgenfeldt, E.R. Weeks, and H.A. Stone, Phys. Rev. E **66**, 040601 (2002).
[33] F. Feuillebois, in *Multiphase Science and Technology*, edited by G.F. Hewitt, J.M. Delhaye, and N. Zuber (Hemisphere, New York, 1989), Vol. 4, pp. 583–798.
[34] H. Tözeren and R. Skalak, J. Fluid Mech. **82**, 289 (1983).
[35] P.J.A.H. Kok, S.G. Kazarian, C.J. Lawrence, and B.J. Briscoe, J. Rheol. **46**, 481 (2002).
[36] B.P. Ho and L.G. Leal, J. Fluid Mech. **65**, 365 (1974).
[37] J.N. Israelachvili, *Intermolecular and Surface Forces* (Academic, London, 1992).
[38] G.E. Yakubov, H.J. Butt, and O.I. Vinogradova, J. Phys. Chem. B **104**, 3407 (2000).
[39] O.I. Vinogradova, G.E. Yakubov, and H.J. Butt, J. Chem. Phys. **114**, 8124 (2001).
[40] G.I. Taylor, *Dispersion of Soluble Matter in Solvent Flowing Slowly Through a Tube* (Cambridge University Press, Cambridge, 1971), Vol. 4, pp. 225–249.
[41] P. Saffman, Q. J. R. Meteorol. Soc. **88**, 382 (1962).
[42] L. Hocking, J. Eng. Math. **7**, 207 (1973).